# Growth temperature effect on physical and mechanical properties of nitrogen rich InN epilayers

Z. Benzarti, T. Sekrafi, A. Khalfallah, Zahia Bougrioua, D. Vignaud, M. Evaristo, A. Cavaleiro

# Growth temperature effect on physical and mechanical properties of nitrogen rich InN epilayers

**Article** *in* Journal of Alloys and Compounds · June 2021

DOI: 10.1016/j.jallcom.2021.160951



**7 authors**, including:

Zohra Benzarti
University of Sfax
**39** PUBLICATIONS **402** CITATIONS
SEE PROFILE

Tarek Sekrafi
CRMN
**7** PUBLICATIONS **23** CITATIONS
SEE PROFILE

Ali Khalfallah
University of Sousse
**67** PUBLICATIONS **291** CITATIONS
SEE PROFILE

Zahia Bougrioua
Université de Lille
**133** PUBLICATIONS **1,822** CITATIONS
SEE PROFILE

# Growth temperature effect on physical and mechanical properties of nitrogen rich InN epilayers

Z. Benzarti[a,*], T. Sekrafi[b], A. Khalfallah[c], Z. Bougrioua[d], D. Vignaud[d], M. Evaristo[c], A. Cavaleiro[c]

[a] Laboratory of Multifunctional Materials and Applications (LaMMA), Department of Physics, Faculty of Sciences of Sfax, University of Sfax, Soukra Road km 3.5, B. P. 1171, 3000 Sfax, Tunisia
[b] Centre de Recherche en Microélectronique et Nanotechnologie, Technopôle de Sousse, BP 334, Sahloul, Sousse, Tunisia
[c] CEMMPRE, Department of Mechanical Engineering, University of Coimbra, Rua Luis Reis Santos, Pinhal de Marrocos, 3030–788 Coimbra, Portugal
[d] IEMN Institute for Electronics, Microelectronics and Nanotechnology, CNRS and Lille University, avenue Poincaré, 59652 Villeneuve d'Ascq, France

Journal of Alloys and Compounds 885 (2021) 160951
https://doi.org/10.1016/j.jallcom.2021.160951

**Keywords:**
InN ; Growth temperature; Surface morphology; Dislocation density; Compressive residual stresses; Nanoindentation

**Abstract**

A set of N-polar InN epilayers has been grown at different temperatures by plasma–assisted molecular beam epitaxy (PA-MBE) on GaN/AlN/$Al_2O_3$(0001) templates. The purpose is to understand how the variation of crucial factor, such as the temperature, impacts the growth process and the resulting samples' properties. The characterization of these InN samples using atomic force microscopy and scanning electron microscopy showed different island distributions and shapes by varying the growth temperature. High resolution-X-ray diffraction (HRXRD) enabled to identify a single crystalline phase (hexagonal wurtzite), whatever the growth temperature. Actually, the increase of growth temperature up to 560 °C has improved the crystalline quality; whereas for high temperature, the crystalline quality degrades. The dislocation density of the epilayer grown at this optimum temperature (around 560 °C) is about $1.9 \times 10^{10}$ $cm^{-2}$, which is determined using HRXRD spectra analysis. High compressive residual stress value of 0.54 GPa was derived using Raman spectroscopy. Room temperature photoluminescence (PL) displays a band gap energy around 0.69 eV. Besides, Burstein-Moss effect, the PL band gap energy measured at 10 K is dictated by the biaxial compressive residual stresses. Nanoindentation tests were carried out on InN epilayers. Only, the sample grown at 560 °C exhibited a pop-in event, for which the measured hardness and Young's modulus are of 4.5 ± 0.5 GPa and of 171 ± 8 GPa, respectively. Accordingly, the growth temperature of InN epilayers influences the resulting physical and mechanical performances, thus a good compromise between physical and mechanical features permits to manufacture efficient devices.

## 1. Introduction

Successful elaboration methods of III-nitride semiconductors GaN, AlN, InN and their alloys contribute to manufacture effective new opto- and micro-electronic devices. Efficient physical properties of such semiconductors are essential for manufacturing effective components, for instance light emitting diodes (LEDs), lasers diodes, UV photodetectors, high electron mobility transistors and more recent highly efficient solar cells [1–4]. However, the successful fabrication of devices based on InN films requires better understanding of mechanical performances along with their physical characteristics.

In the past few years, researchers have devoted and even increased efforts to study InN properties. They fortunately discovered its effective narrow band gap energy of 0.7 eV for single crystals with high electron carrier density (from $2 \times 10^{18}$ $cm^{-3}$ to $10^{21}$ $cm^{-3}$) [5–8] instead of 1.9 eV for polycrystals with electron carrier density that can vary between $10^{16}$ $cm^{-3}$ to $10^{21}$ $cm^{-3}$ [9,10]. The origin of noticed InN band gap energy difference was explained by the very high electron carrier density in the material and the subsequent band filling [11]. Based on first-principle calculations, Liu et al. [8] have shown that *n*-type defects, such as substitutional oxygen on the nitrogen site ($O_N$), nitrogen vacancies ($V_N$) and substitutional silicon on the indium site ($Si_{In}$) are responsible for the blue shift of InN absorption edge. These defects contribute to increase the free electron density, owing to their low formation and ionization energies. The Burstein-Moss (BM) shift enlarges the optical band gap [12,13]. Later on, it has been found that strains can also contribute to the variation of the band gap [14,15]. Both contributions of BM and

* Corresponding author.
*E-mail address:* zohra.benzarti@fss.usf.tn (Z. Benzarti).

strains were also observed in GaN films with various thickness and different silicone doping [16–18].

Among III-V nitrides fabrication processes, the growth of InN is the most challenging one. Indeed, the large lattice mismatch between $Al_2O_3$ sapphire substrate and InN (about 25%) is a concrete impediment for InN growth process. Despite this fact, InN films are commonly grown on $Al_2O_3$ sapphire substrates, as they are abundantly available, simple to handle and featured by hexagonal crystalline symmetry. Nonetheless, the usage of more appropriate buffer layer is necessary to reduce the residual crystal stresses originated from lattice mismatch $Al_2O_3$ substrate/InN. GaN and AlN buffer layers are frequently used to grow InN layers despite the existence of a lattice mismatch of 11% and 13%, respectively [19,20]. Currently, InN growth layers on c-oriented sapphire substrate is mainly carried out using GaN intermediate buffer layer. The low dissociation temperature is regarded as an extra serious problem for effective InN growth process. In fact, to obtain high-quality InN films, two parameters must be monitored and optimized: (i) the growth temperature that should be set as higher as possible, but without reaching InN dissociation temperature; (ii) the V/III ratio should be accurately controlled to grow N-polar InN films [21]. As a result, low temperature in the range of (460–550 °C) was used for successful epitaxial growth of InN films [22]. Moreover, for effective InN film epitaxy, the maximum growth temperature influences the film polarity [23]. It was reported that N polar InN films could be grown at about 100 °C higher than In-polar ones [24]. As commonly known, high growth temperature of III-nitrides, including InN films, is essential for the fabrication of high crystalline quality device structures. In fact, Zhang et al. [25] indicated that the temperature growth higher than 575 °C is favourable for the epitaxy of high InN hexagonal purity. Wang et al. [14] reported that the growth temperature ranged between 540 °C and 600 °C was recommended for N-polar InN epitaxy.

On this basis, we elaborated InN epilayers at three temperatures, namely: 530 °C, 560 °C and 590 °C. The latter temperature is close to the limit temperature of the dissociation of N-polar InN epilayer. In literature, several physical properties of InN films have been reported [9]; however, it is also vital to investigate the effect of growth mechanisms, and particularly the growth temperature on the characteristics of InN films. The assessment of the mechanical properties of semiconductors, such as hardness and Young's modulus, are likewise of paramount importance as the physical features, for successful fabrication of InN-based devices. The contact loading and/or packaging that can experience during fabrication could really damage the devices' performance. Nanoindentation technique is currently an effective method for probing mechanical features of thin films at nanoscale, without any concern about the limitation of sample size and shape [26]. However, it is noticed a large dispersion of the measured mechanical properties that were reported in literature [26–28]. This discrepancy is likely explained by the different growth methods used for InN epitaxy, the dissimilar growth conditions, the various InN thickness layers studied and the shape and indenter tip radius used in nanoindentation tests. For PA-MBE epitaxial technique, to procure the optimal growth temperature is crucial for the elaboration of high-quality InN thin films, and then to obtain competitive physical and mechanical properties of InN-based devices.

In this paper, we report the growth temperature effect on morphological, microstructural, electrical, optical properties and mechanical characteristics of N-polar InN epilayers. A set of similar-thick InN epilayers were grown on GaN/AlN/$Al_2O_3$(0001) template using plasma assisted molecular beam epitaxy (PA-MBE). The physical and mechanical properties of N-polar InN epilayers were assessed and analysed. We conclude on the optimum growth temperature and providing related results.

## 2. Experiment

InN samples were grown on c-(0001) $Al_2O_3$ substrate by PA-MBE. AlN nucleation layer 20 nm-thickness was initially deposited on the substrate at 800 °C, followed by a 2 µm thick GaN buffer layer at 700 °C. AlN nitridation of sapphire is very effective for producing single crystals. Finally, 300 nm thick InN epilayers were grown at three temperatures, namely: 530 °C, 560 °C and 590 °C, denoted by sample (A), (B) and (C), respectively. The substrate temperature was measured by an SVT associates in situ 4000 process monitor based on emissivity-corrected pyrometry. InN epilayers were deposited using 2.2 sccm $N_2$ flow rate, which produced a pressure of $10^{-5}$ Torr, and 740 °C indium effusion-cell temperature. The effective V/III ratio was carefully monitored by changing the radio-frequency (RF) plasma power between 230 W and 250 W. In these conditions, the effective In/N ratio was almost equal to unity and it was slightly N-rich. After growth, no metal droplet on sample's surface was perceived. The N-polar InN growth rate, which dictates the InN thickness layer, increased slightly along with the increase of the growth temperature [29]. In order to obtain alike InN sample's thickness, for the different growth temperature, the power was controlled to keep InN growth rate around 200 $nm.h^{-1}$. This growth rate was chosen to avoid In-droplets as reported by Gallinat et al. [30].

Zeiss Merlin high resolution Field Emission Scanning electron microscopy (FE-SEM) equipped with Bruker QUANTAX EDS-Detector was used to observe and analyse images of the three sample surfaces to reveal the growth temperature effect on the surface morphology of InN epilayers. The vacuum chamber pressure was set to about $2.10^{-4}$ Pa and utilizing an acceleration voltage of 2 kV. Image magnification was set between 20 k x and 35 k x and In-lens Energy-selective-Backscatter (EsB) detector was used and 750 V for the grid voltage. Before SEM image processing, samples were cleaned in acetone. In addition, Nanoman AFM (atomic force microscope), controlled by a Nanoscope V electronics from Bruker Instruments, was used to perform AFM analysis of the surface morphology of InN epilayers in tapping mode by carrying out 2 µm x 2 µm scans using a cantilever with a nominal tip radius between 2 and 5 nm (Nanosensors NCL tip).

The growth of single-crystalline c-(0001) oriented hexagonal InN epilayers were confirmed by HRXRD measurements using the Cu-Kα1 radiation. (0002), (0004) and (0006) rocking curves were obtained using Williamson-Hall plots to deduce the screw dislocation density [31]. Then, (0002), $(10\bar{1}3)$, $(10\bar{1}2)$, $(10\bar{1}1)$ and $(30\bar{3}2)$ reflections were used to determine the edge dislocation density [16]. Compressive residual stresses are probed using room temperature micro-Raman spectroscopy. Hall Effect measurement at room temperature was achieved, in order to evaluate electrical properties.

Photoluminescence (PL) measurements were performed at 10 K and at room temperature using 488 nm argon laser, which penetrates around 100 nm of InN film depth, with 40 mW power excitation and an extended range InGaAs detector.

The mechanical properties of InN epilayers were extracted using nanoindentation technique. Indentation tests were carried out using nanoindentation instrument (NanoTest NT1, NanoMaterials, Ltd) equipped with a diamond pyramid-shaped Berkovich-type indenter of 100 nm curvature tip radius. The load rate-control mode up to the maximum loads $P_{max}$ of 2 mN. Each load-unload duration was kept for 30 s 16 indents were performed and each indentation was separated by 30 µm to avoid measurement interferences. From the load-displacement results, the hardness (H) and Young's modulus (E) of InN epilayers were determined using Oliver and Pharr method [32]. The imprint of 150 mN Nanoindentation maximal load is shown in SEM image as pointed by narrows (see, Fig. 1).

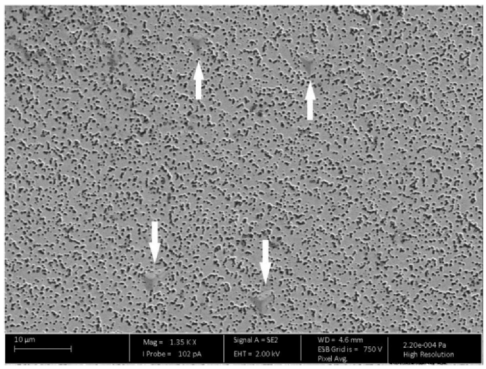

**Fig. 1.** SEM image of the imprint of 150 mN Nanoindentation maximal load, pointed by narrows, for sample B (560 °C).

## 3. Results and discussion

Fig. 2 shows AFM images that describe the evolution of the surface morphologies with the growth temperature for the three N-polar InN samples (A), (B) and (C) grown at 530 °C, 560 °C and 590 °C, respectively. It clearly displays the important influence of temperature on surface morphology. This is probably due to the change of the growth mode [33]. The surface of sample (A) shows tiny grains, which is likely owing to low surface migration occurred at lower temperature (530 °C) compared to the growth temperature of the other samples. The sample (B) presents facets, which are similar to hexagonal shapes and large islands. This may be due to the increase of diffusion length, when the growth temperature was raised [34]. Zhang et al. [25] reported that the high temperature growth (about 575 °C) promotes the formation of high hexagonal purity InN film. According to this, it seems that, the sample (B) is experienced the stage of lateral coalescence of large island layers and likely promoting for a better crystalline quality. In addition, the large islands are featured by wide grain boundaries, which probably would be the origin of low-density edge-type dislocations forecasted for the sample (B).

AFM image for sample (C), shows large clusters of grains (see Fig. 2c) that are formed probably due to the decomposition or thermal etching of InN epilayer at high temperature. These clusters of grains have almost similar dimension as that for sample (B). However, they do not present facets and this may be indicative that at 590 °C growth temperature, the morphology starts to degrade and to suffer a pre-dissociation phenomenon [29]. This presumably could lead to a poor crystalline quality, as Zhang et al. [35] reported. Fig. 3 shows SEM images for the three InN samples, where it shed some lights on the surface morphology changes originated from the growth temperature. Chiefly, it is interesting to figure out that Fig. 3b depicts, for sample (B), the surface morphology of large 2D islands layer with approximately hexagonal shape undergoing coalescence phase along the InN growth process at 560 °C. Truncated smooth surfaces of these large islands are very visible. For such morphology, one can expect that, with thicker InN epilayer than sample (B), a smoother epilayer would be accomplished with enhanced crystalline

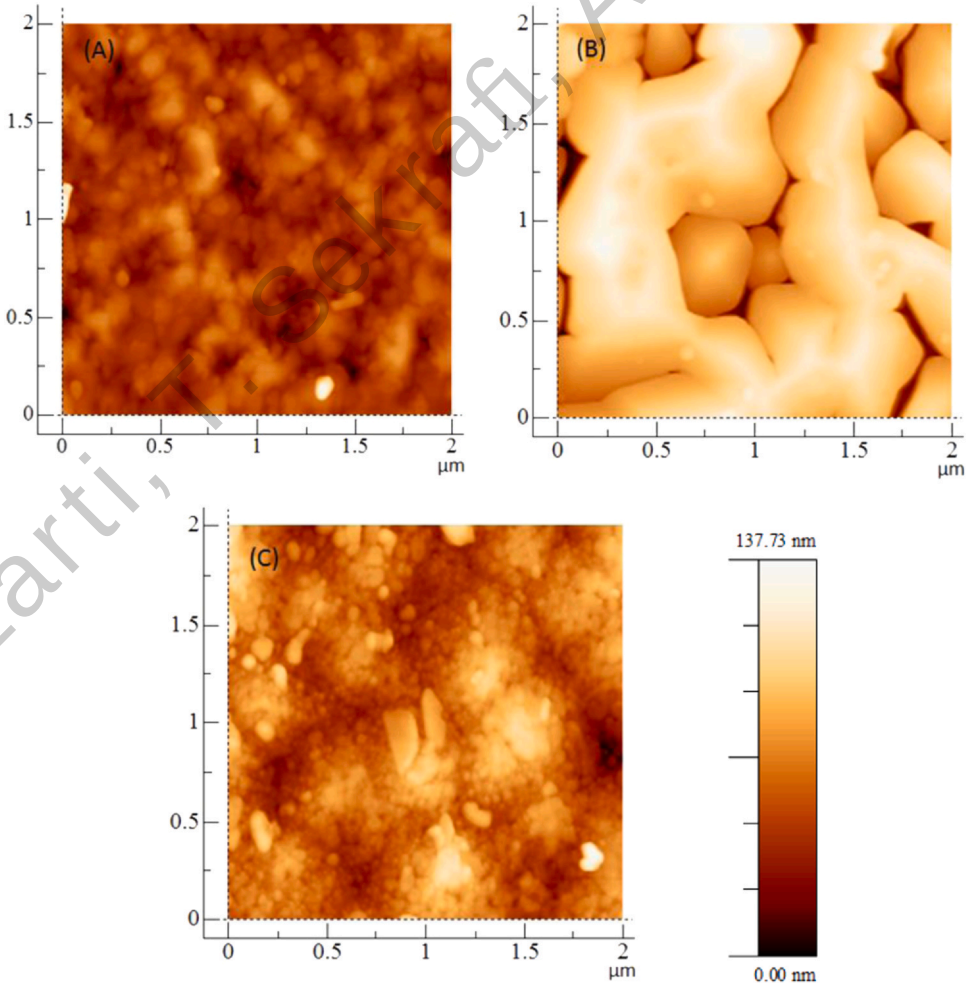


**Fig. 2.** 2 × 2 µm$^2$ AFM images of InN samples grown at: (A) 530 °C, (B) 560 °C and (C) 590 °C.

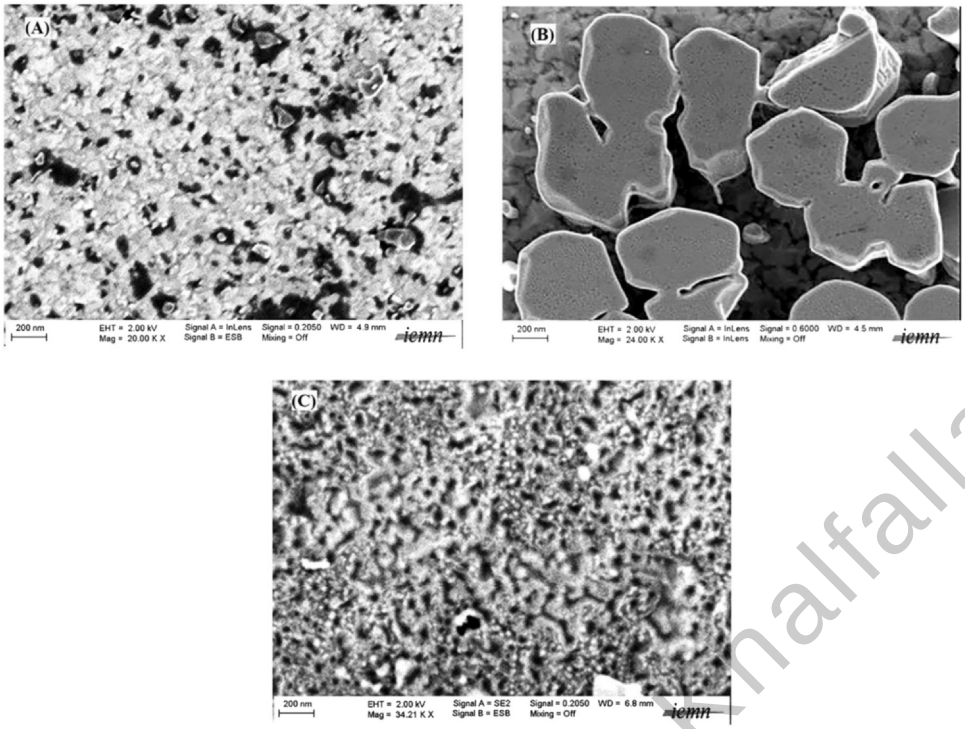


**Fig. 3.** SEM images of three InN samples grown at: (A) 530 °C, (B) 560 °C and (C) 590 °C.

quality. However, the surface morphology for both InN epilayers (A) and (C) are featured by a high surface roughness (see Fig. 3a and c). Accordingly, the SEM images are found in accordance with the AFM analysis.

Fig. 4 displays typical ω/2θ X-ray diffraction spectra of the three N-polar InN heteroepitaxial layers grown at different temperatures. InN (0002), GaN (0002), AlN (0002) and $Al_2O_3$ (0006) diffraction peaks are observed at 31.4°, 34.5°, 36° and 41.7°, respectively. The peaks at 2θ = 65.38° and 72.75° correspond to the InN (0004) and GaN (0004) reflections, respectively. This is indicative of [0001] oriented hexagonal single crystal InN epilayers. The comparison of the spectra clearly shows that the peak intensities are maximum for InN sample (B). The sample (C) shows lower intense InN (0002) peak and its (0004) peak is absent, indicating a low crystalline quality of this film grown at 590 °C. One can notice that there is no indication of metal-indium in all InN samples; otherwise, this results in the observation of In (101) diffraction peak around 33°. Such results, shows indirectly that the dissociation temperature of N-polar InN epilayer was not yet reached. Actually, as it has been reported, the InN decomposition could occur for a growth temperature higher than 600 °C [35,36]. Wang et al. [37] reported that the dissociation temperature of InN is lower than the desorption temperature of In metal.

In order to assess the structural quality of InN epilayers, we proceed by the comparison of the intensity and the full width at half-maximum (FWHM) of the X-ray rocking curves of the (0002) InN reflections, as presented in Fig. 5. The growth temperature has a significant impact on the peak intensity and FWHM. Sample (B) rocking curve displays the highest and narrowest InN (0002) peak, which indicates that, in these epitaxial conditions, the growth temperature 560 °C is the optimum temperature. On the other hand, the c-lattice constant of the three samples can be extracted using X-ray rocking curves of the (0002) InN reflections. The c-lattice parameter rises along with the increase of growth temperature until 5.718 Å for sample (B), then decreases. It is found that this parameter evolves between 5.705 Å and 5.718 Å, when the growth temperature drops from 590 °C to 560 °C, respectively, as reported in Ref. [14]. Given that N-polar InN unstrained lattice constant is $c_0$ = 5.7033 Å,

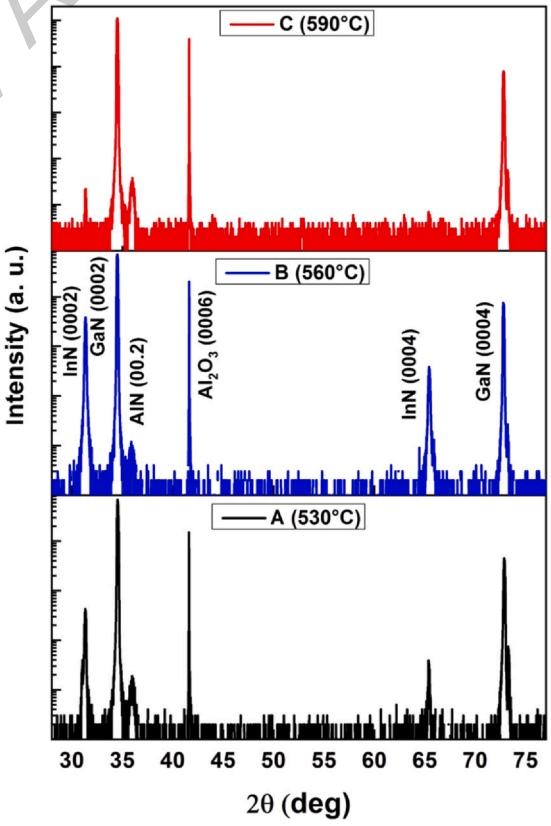


**Fig. 4.** X-ray ω/2θ scans of InN epilayers deposited on GaN/AlN/sapphire templates with different growth temperatures.

thus, the three InN epilayers (A, B and C) incur compressive residual stresses.

To further get insight into the microstructure temperature-dependent evolution, it is possible to estimate from HRXRD the screw

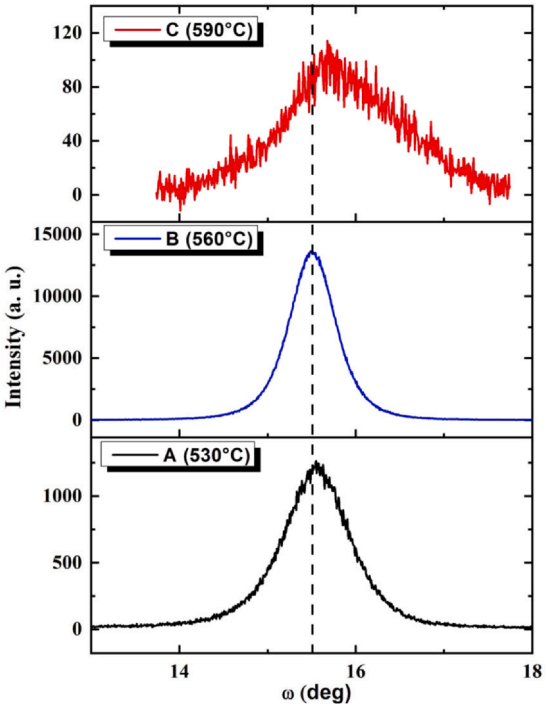


**Fig. 5.** (0002) ω scan of InN epilayers for samples A, B and C.

and edge dislocation densities of single crystalline layers that present a certain degree of mosaicity. InN growth is characterized by the nucleation of disoriented islands that can proliferate the dislocation merging from underlying threading dislocations within the template [38,39] and new threading dislocation density is generated at the coalescence joints. Therefore, it is expected that larger threading dislocation density within InN film is higher than that within GaN template. Some examples of dimension and angular distribution of mosaic domains in InN epilayers were for instance reported in [40]. The size of InN domains can be described by lateral ($L_{//}$) and vertical ($L_{\perp}$) coherence lengths. The screw and edge components of the dislocation Burger vector are associated to the tilt ($\alpha_{tilt}$) and to the twist ($\alpha_{twist}$) angles, respectively. The average values of the tilt and twist are related to the FWHM of the symmetric and asymmetric rocking curve, respectively [41]. It is worth to note that the calculated screw or edge dislocation densities, obtained from diffraction measurements, correspond to the sum of two densities: pure screw and mixed dislocations or pure edge and mixed dislocations. Essentially, only a direct analysis by Transmission Electron Microscopy (TEM) would accredit the real distribution of screw, edge and mixed dislocations.

The broadening of the rocking curve (ω scan) of the (0002), (0004) and (0006) reflections is affected by the tilt and lateral coherence lengths, as measured by triple axis X-ray diffraction. Fig. 6 depicts Williamson-Hall plots [31] that show the evolution of FWHM*(sinθ)/λ versus (sinθ)/λ for samples (A) and (B); where θ is the Bragg angle and λ is the X-ray wavelength. For sample (C), it was impossible to detect the (0004) and (0006) reflections because of its low crystalline quality. The y-intersection of each linear fit gives the lateral coherence length: $L_{//}$ = 79 nm and 110 nm, respectively for samples (A) and (B). The larger lateral coherence length found for sample (B) is consistent with our AFM observation of larger grains. From the slope of the same plots, $\alpha_{tilt}$ was determined to be 0.8° and 0.4° for samples (A) and (B), respectively. This confirms that sample (B) is less defective than sample (A).

By using the following equation, the screw-like dislocation density is derived [42]:

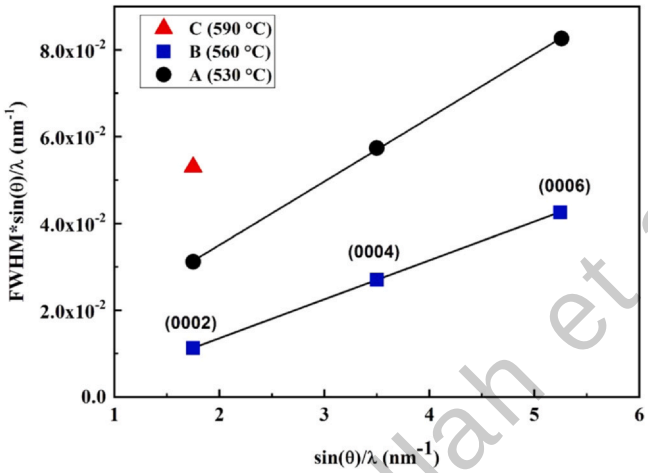


**Fig. 6.** Williamson-Hall plot for triple-axis ω scans of (0002), (0004) and (0006) InN symmetric reflections.

$$N_{screw} = \frac{\alpha_{tilt}^2}{4.35\ b_c^2} \quad (1)$$

where $b_c$ is the Burgers vector of c-type threading dislocations ($b_c$= c = 0.5705 nm for InN [43]), we can deduce the screw-like dislocation density ($N_{screw}$): (1.9 ± 0.1)x$10^{10}$ $cm^{-2}$ and (5.1 ± 0.2)x$10^{9}$ $cm^{-2}$ for samples (A) and (B) InN epilayers, respectively. The screw dislocation density of sample (A) is clearly higher than that of sample (B); as it has been anticipated. This confirms the higher crystalline quality of sample (B) compared to other samples.

For the estimation of the mosaic twist, the FWHM of (0002), (10$\bar{1}$3), (10$\bar{1}$2), (10$\bar{1}$1), and (30$\bar{3}$2), reflections were measured with increasing lattice plane inclination Ψ. Only the spectra of sample (B) could be analysed suitably (see Fig. 7). But, because of the poor crystalline quality of sample (A), it was very arduous to accurately measure the FWHM from rocking curves for some asymmetric peaks that were somehow flattened. Thus, it was impossible to completely plot FWHM as function of Ψ angle and therefore to determine the twist angle for sample (A). Furthermore, the low crystalline quality of sample (C) was likely the main impediment cause to measure any of its asymmetric signal. The measurements related to sample (B) could be fitted using the Srikant et al. model [41]. The extrapolation of the fitting curve (open squares) to the inclination angle of 90°

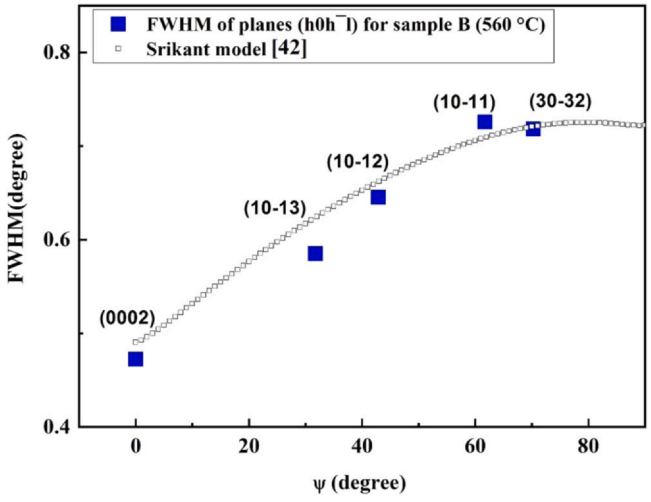


**Fig. 7.** Variation of the FWHM of peaks corresponding to asymmetric planes ($h0\bar{h}l$) as a function of inclination angle for sample B. The open square line is the experimental point fit using Srikant model [42].

corresponds to the mosaic twist angle. The obtained twist angle ($\alpha_{twist}$) is about 0.7° for sample (B). The Fewster model permits to deduce the density of edge-type dislocations [44]:

$$N_{edge} = \frac{\alpha_{twist}}{2.1|b_a|\ L_{//}} \quad (2)$$

where $b_a$ is the Burgers vector of a-type threading dislocations ($|b_a|$= a = 0.3525 nm for InN [43]). Thus, the calculated edge-like dislocation density is (1.41 ± 0.05)x$10^{10}$ $cm^{-2}$ in sample (B). It is almost 4 times higher than the screw dislocation density for the same layer. It is known that mixed dislocation density consisting of both screw and edge character, and if we assume that c-plane GaN layers, the pure-screw dislocation density is very low compared to the edge and mixed dislocation densities, thus we can infer the values for mixed dislocation density and pure-edge dislocation density of about $5.1 \times 10^9$ $cm^{-2}$ and $1.4 \times 10^{10}$ $cm^{-2}$, respectively. These dislocation density values are in accordance with the state-of-the-art findings published. The pure-edge dislocation density is lower than in MBE grown InN layers of Darakchieva et al. [45] ($1.9 \times 10^{10}$ $cm^{-2}$ - $3.4 \times 10^{10}$ $cm^{-2}$). Dimakis et al. [46] have observed by TEM a very thick InN MBE grown layer (10 µm) and has found a comparable value of the pure edge dislocation density ($1.5 \times 10^{10}$ $cm^{-2}$) in the InN/GaN interface region, whereas, the dislocation density value is decreased around ($4.3 \times 10^9$ $cm^{-2}$) vicinity of the InN free surface. Moreover, Liu et al. [40] used the similar models and formulas as those used in the present work and they found that the edge dislocation density was round $4.0 \times 10^9$ $cm^{-2}$ within 10 µm MBE InN film thickness and $2.1 \times 10^{10}$ $cm^{-2}$ within 600 nm MOCVD InN film thickness. Therefore, the growth process (method and growth conditions), along with the thickness of InN films could be considered as one of the most influential factors on the dislocation density generated in samples. Hence, the discrepancy between dislocation densities reported in Ref. [40] and those presented in this work is mainly attributed to the dissimilarity in film thicknesses, (i.e. the thickness of sample (B) is by far thinner than the one reported in Ref. [40]). As referred by Gallinat et al. in Ref. [30], the threading dislocation density increases sharply for InN thickness lower than 1 µm. Therefore, the screw and edge dislocation densities obtained for the sample (B) of 300 nm thickness reflect its crystalline quality.

Raman scattering from the samples showed useful information about the InN phonon modes could be extracted. Fig. 8a shows Raman spectra of the three samples (A, B and C) which are grown on GaN templates. Many distinct peaks were obtained around the positions of 143 $cm^{-1}$, 418 $cm^{-1}$ and 569 $cm^{-1}$ which correspond to the $E_2$(low), $A_1$(TO) and $E_2$(high) GaN phonon modes, respectively. In addition, two distinct peaks were detected about 492 $cm^{-1}$ and 592 $cm^{-1}$ which agree with $E_2$(high) and $A_1$(LO) InN phonon modes, respectively. Two-star marks are localized at 380 $cm^{-1}$ and 415 $cm^{-1}$ positions associated to Raman modes of sapphire substrate.

Due to its non-polar nature, the $E_2$ (high) phonon mode is not affected by the electron carrier density and it is regarded as the best method to assess the residual stresses and crystalline quality of the deposited films. Moreover, native defects influence the FWHM broadening of the $E_2$(high) mode [47]. Relatively to the InN $E_2$ stress-free frequency (491.1 $cm^{-1}$), a blue shift in the $E_2$(high) mode frequency is a result of compressive residual stresses within InN epilayers. The inset of Fig. 8a reveals that the three samples (A, B and C) have compressive residual stresses. Particularly, the sample (C) shows the less compressive residual stress, owing to the experienced plastic relaxation. Such conclusion is confirmed by AFM image analysis and HRXRD measurements, where the increase of threading dislocation density and the drops of its c-lattice parameter were noticed. In addition, sample (B) has the narrowest FWHM confirming its best crystalline quality, which is correlated with HRXRD results. Quantitatively, the residual biaxial stress $\sigma$ of InN thin films is

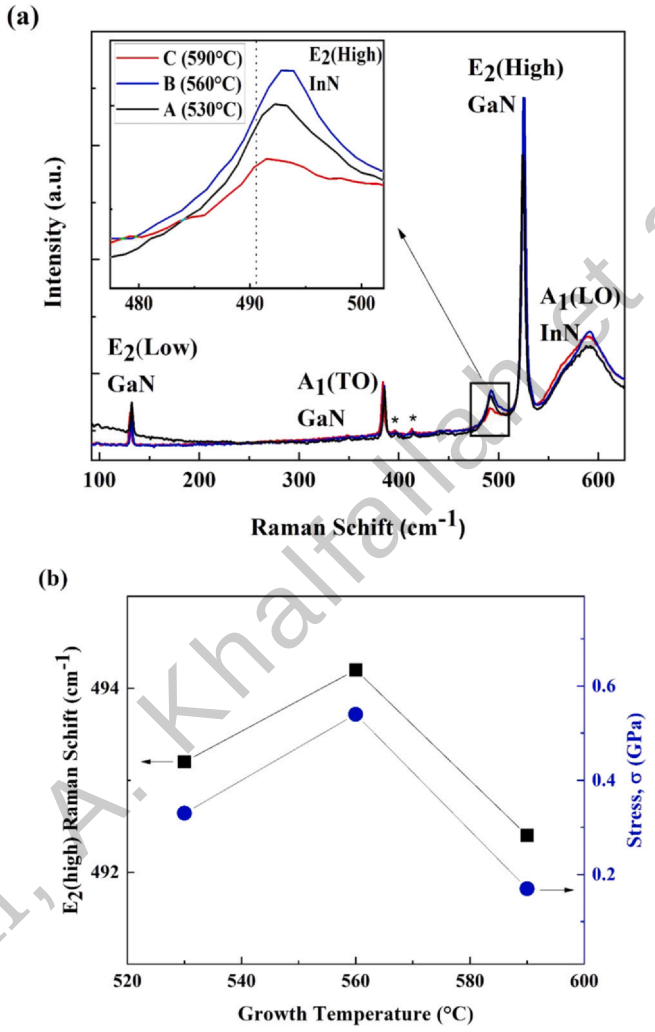


**Fig. 8.** (a) Raman spectra of N-polar InN epilayers grown at different temperatures. The inset depicts the shift of $E_2$(high) peak versus the growth temperature; (b) The dependence of E2(high) mode frequency (black solid rectangular) and the compressive residual stresses (blue solid circle) versus the growth temperature.

related to the frequency of $E_2$(high) mode by the following equation [48]:

$$\sigma(GPa) = 0.18 \times (\omega - 491.1)(cm^{-1}) \quad (3)$$

Fig. 8b shows the frequency of $E_2$(high) mode and residual stress for the different growth temperature. One can see that the residual stress increases from 0.33 GPa to 0.54 GPa for arise of the growth temperature from 530 °C to 560 °C, respectively. Then the stress decreases to 0.17 GPa for 590 °C growth temperature. These results are in accordance with the obtained dislocation density. In fact, the higher dislocation density, the lower residual stress is (sample C).

Fig. 9 depicts, for (A), (B) and (C) samples, the obtained electrical properties using Hall Effect measurements at room temperature. All films show *n*-type conductivity. The origin of the electrons is attributed to nitrogen vacancies ($V_N$) generated by the low cracking efficiency of ammonia [49] or by the high growth temperature [47]. The electron carrier density is around $3 \times 10^{18}$ $cm^{-3}$ for the three N-polar InN samples. In the range from 530 °C to 590 °C of growth temperature, *n*-type carrier density varies slightly. Meanwhile, the electron carrier mobility increases from 24 to 240 $cm^2$/V.s. It was agreed that the dislocations have strong effect on the electron carrier mobility. Thus, in this context, the increase of the growth temperature achieves the enhancement of electron carrier mobility by a factor of 10. This is owing to the improvement of the crystalline

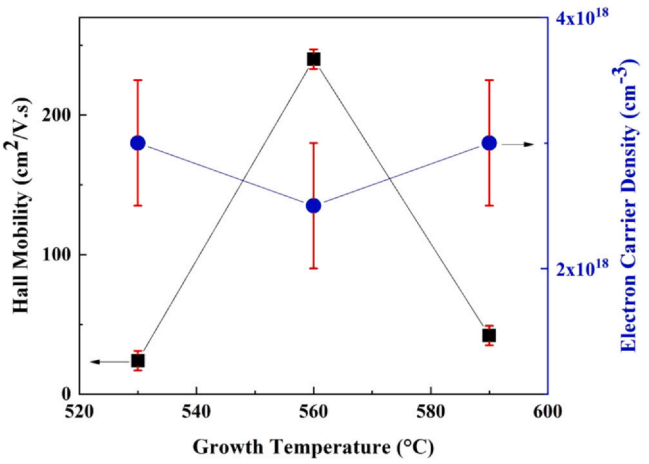


**Fig. 9.** Room temperature InN Hall mobility (black solid rectangular) and electron carrier density (blue solid circle) as function of InN growth temperature. Errors correspond to the red bar size.

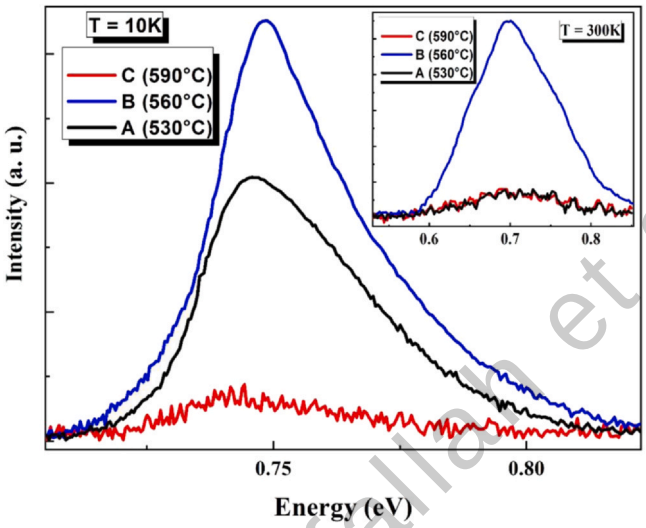


**Fig. 10.** PL spectra performed at 10 K of N-polar InN epilayers elaborated at different temperatures. The inset represents room temperature PL spectra.

quality and to the diminution of threading dislocation density as proved above. It was reported by several research groups that the decrease of edge type dislocations leads to the increase of the electron carrier mobility [50]. The thickness also influences the electrical properties of N-polar InN thin layer. In fact, Liu et al. [51] reported the effect of thickness on electrical properties of InN layer of about 200 nm thick. They found mobility value (235 $cm^2$/V.s) comparable to that was obtained for the sample (B). The improvement of electron carrier mobility for sample (B) is accredited to its high crystalline quality. In addition, the morphology of sample (B) with large islands is suitable for the increase of its electron carrier mobility. This same behaviour was observed by Lai et al. [52] in the range of temperature of 500–560 °C, the electron carrier density remains almost constant, whereas the carrier mobility increases vastly (10 times). Likewise, Lu et al. [53] obtained a low evolution of electron carrier density around $7 \times 10^{18}$ $cm^{-3}$ in the range of growth temperature of 500–600 °C, contrary to carrier mobility, which varies between 150 $cm^2$/V.s to 350 $cm^2$/V.s.

It is noticed a significant decrease of the carrier mobility (42 $cm^2$/V.s) at growth temperature of 590 °C (sample C). This drop of electrical properties might be assigned to the poor crystalline quality. It is worth to note that the carrier mobility of sample (C) (42 $cm^2$/V.s) is higher than that of sample (A) (24 $cm^2$/V.s). This is probably owing to the high growth temperature, which causes large clusters of grains observed on the surface of sample (C).

Fig. 10 shows PL spectra of the three N-polar InN epilayers (A, B and C) recorded at 10 K. One can see that the luminescence of sample (A) and sample (B) is solely noticeable. This approves the degradation of crystalline quality of sample (C) grown at high temperature (590 °C). In addition, the sample (B) (grown at 560 °C) shows the highest intensity with the smallest FWHM. This result confirms the best optical quality of this sample, which is attributed to its high crystalline quality along with its low threading dislocation density.

The inset of Fig. 10 shows room temperature PL spectra of the three N-polar InN epilayers. It is worth to notice that low luminescence is observed for the samples (A) and (C) which is due to the vanished optical quality of these samples at room temperature. This could be explained by the high defect density, where the obtained threading dislocation density for sample (A) was found at least 3 times higher than that within sample B. Zhang et al. [25] reported that for MOVPE InN samples grown at low temperatures, there was cubic phase inclusion into the hexagonal phase. The luminescence quenching can be related to the cubic InN domains as well as to the extended defects, such as threading dislocations. For sample (C) grown at 590 °C, the desorption of N combined with the extended defects are the main causes for its low luminescence.

For sample (B) high PL intensity is observed, which can be attributed chiefly to its high crystalline quality and thus to its low defect density. It is worth to note that room temperature PL spectrum for sample (B) exhibits single emission energy near 0.69 eV associated to the near-band-edge emission [54]. The comparison between the PL spectra of sample (B) recorded at room temperature and at low temperature, reveals that the band edge emission undergoes a redshift and broadens by increasing temperature from 10 K to 300 K. The lattice expansion and electron-phonon interaction are the origin of such behaviour.

On the other hand, the shift of the band gap energy shows the same evolution observed in Raman spectra. In fact, sample (B) reveals a blue shift both for the band gap energy and the $E_2$(high) Raman peak indicating the increase of compressive residual stresses. In addition, the blue shift of the band gap energy can be caused by the Burstein–Moss (BM) effect, which plays a crucial role on the optical properties of InN films owing to the presence of high electron carrier density [47]. Song et al. [55] reported that band filling and band gap renormalization contribute to the evolution of PL band gap energy with changing electron carrier density. But, the electron carrier density is almost the same for all studied samples (A, B and C). Therefore, besides to BM effect, the observed PL band gap energy shift is governed by compressive residual stresses. This is confirmed by the shape of PL band gap peak. Contrary to our case, Wang et al. [14] reported that the tails at the lower energy side are related to band filling effect. Wen et al. [56] studied the growth temperature effect on optical response of GaN thin films grown by MBE and they obtained a blue shift at the beginning, then the PL peak of band edge regresses along with the increase of the growth temperature. Moreover, the growth temperature affects the FWHM of PL band gap peak at 10 K. This FWHM evolution is related to the threading dislocation density. The lowest FWHM (17 meV) is obtained for the sample (B), which has the highest carrier mobility (240 $cm^2$/V.s) and the lowest threading dislocation density.

In order to assess mechanical properties of N-polar InN epilayers grown at different temperature, nanoindentation tests were performed at room temperature with 2 mN as maximum load. Fig. 11, shows the effect of growth temperature on the load-displacement curves of N-polar InN epilayers (A, B and C). Each load-displacement curve represents an average of 16 nanoindentation tests. The maximum penetration depth into (A), (B) and (C) InN epilayers is about

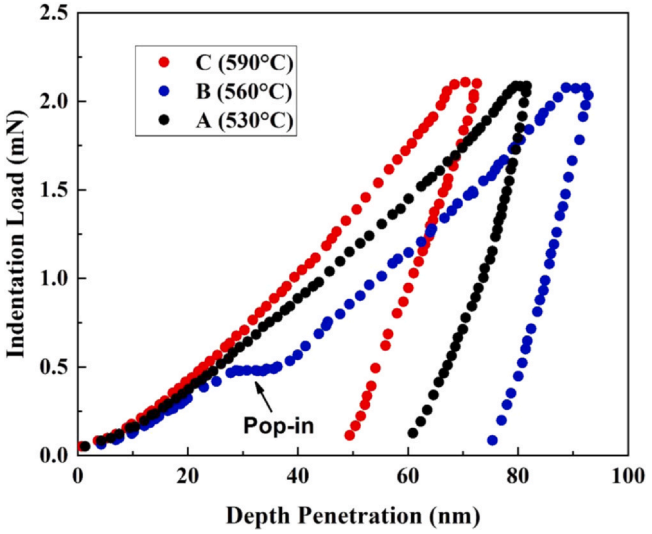


**Fig. 11.** Average of 16 load-displacement curves of InN epilayers grown at different temperature. During loading, pop-in event is only depicted for sample B (560 °C).

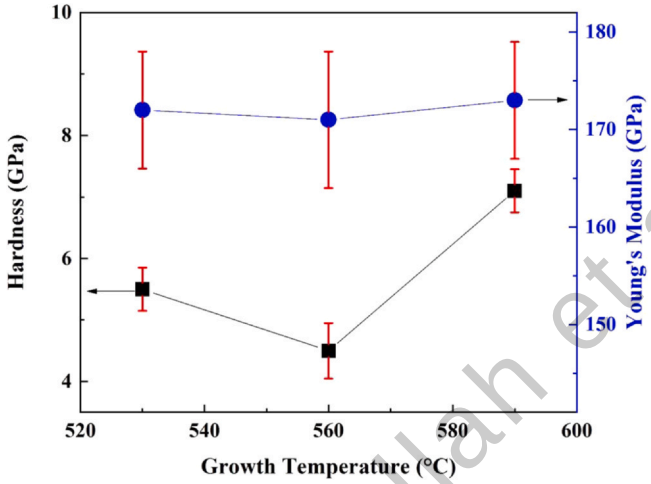


**Fig. 12.** Variation of nanoindentation hardness (black solid rectangular) and Young's modulus (blue solid circle) as function of InN growth temperature. Errors correspond to the red bar size.

80 nm, 90 nm and 70 nm, respectively. These depths respect the nanoindentation criterion proposed by Li et al. [57] to avoid the effect of the substrate mechanical properties on the indented samples. This means that, the nanoindentation depth should never exceed 30% of the film thickness. Our results are comparable to that obtained by Jian et al. [24], where almost similar penetration depths with 1 mN maximum load for 300 nm InN thin layer were found. Kataria et al. [58] reported that the growth orientation of sapphire has an effect on mechanical properties of 700 nm InN film. In fact, c-(0001) sapphire orientation nanoindentation curve shows the appearance of pop-in event around 0.6 mN as critical load and 50 nm as penetration depth. The maximum penetration depth into InN epilayer is about 100 mN for 2 mN as maximum load and its hardness is about 8 GPa. The pop-in event is related to the mechanism of homogenous dislocation nucleation of loops during nanoindentation. It is observed only for sample (B) at 0.5 mN as critical load and 28 nm as penetration depth. The origin of discrepancy between indented InN samples is not clear at present. However, one can assume that the plastic-induced deformation mechanism is not similar for these samples. Such behaviour could be likely related to difference of the residual dislocation density found in the grown samples. Therefore, the interactions of these dislocations with the indenter tip are unalike. Fig. 12 displays the hardness and Young's modulus for the different samples grown at the aforementioned temperatures. It is worth to notice that the hardness varies between 4.5 ± 0.5 GPa and 7.1 ± 0.4 GPa depending on the growth temperature; however, the Young's modulus is just about a constant value of 171 ± 8 GPa. These mechanical properties are close to that obtained by Ohkubo et al. [59] who investigated InN thin films of 0.5–4 μm thickness grown by MBE method. The hardness and Young's modulus were determined to be 8.2 GPa and 178 GPa, respectively. They reported that mechanical properties were strongly affected by the InN crystallinity.

For our samples, the minimum value of hardness was found for sample (B), which has less residual dislocation density with more compressive residual stresses. In fact, during the nanoindentation load, the tip indenter interacts with pre-existing dislocations and defects at the sample surface. Thus, residual dislocations resist to the indenter penetration in a collective way then the hardness increases. But, since the InN material is featured by ductile behaviour (as sample (B)), the indenter easily penetrates into the layer containing small amount of residual dislocations and then the obtained hardness value is the smallest. There may be generate additional dislocations which propagate in the form of loops underneath the indenter tip creating pop-in events due to homogenous nucleation and propagation of dislocations and announcing the elastoplastic transition behaviour of the stressed volume underneath the tip indenter.

In addition, sample (A) and (C) don't show pop-in events and they are harder than sample (B). For sample (C) grown at 590 °C, which has poor morphology and low crystalline quality result of predissociation phenomenon, the hardness is the highest. In fact, (0002) X ray rocking curves exhibit the highest residual dislocation density and less compressive residual stresses as shown by Raman results for sample (C). Subsequently, we can conclude that the reduction of compressive residual stresses induced by the plastic relaxation at the same time of the increase of pre-existing dislocation density are responsible for the revealed hardness increase and the absence of the pop-in events in InN samples grown at 530 °C and 590 °C.

## 4. Conclusion

N-polar InN epilayers were grown at 530–590 °C temperature range (i.e., below the dissociation temperature) using MBE technique. The elaborated structures have been characterized by AFM, SEM, HRXRD, Van der Pauw Hall Effect, Raman, PL techniques and nanoindentation method to probe mechanical features. Our aim is to understand the effect of growth temperature on the physical and mechanical properties. A strong temperature dependence of the mosaic structure in single crystalline phase (hexagonal wurtzite) InN epilayer is shown. Morphology, FWHM of X-ray rocking curves, electron carrier mobility, compressive residual stresses, PL intensity at 10 K and room temperature vary along with the growth temperature. These analyses clearly indicate that the improvement of InN physical quality can be achieved using an optimal growth temperature 560 °C, for which the threading dislocation density is the lowest ($1.9 \times 10^{10}$ $cm^{-2}$) with highest compressive residual stresses value (0.54 GPa). In this growth condition, the band edge emission of the epitaxial InN epilayer is 0.69 eV at room temperature.

The various growth temperature revealed an important impact on the mechanical properties, in particularly, the hardness which varies between 4.5 ± 0.5 GPa to 7.1 ± 0.4 GPa; whereas Young's modulus fairly remains around 171 ± 8 GPa. Pop-in event with 0.5 mN as critical load was observed only in InN epilayer grown at 560 °C. Subsequently, we obtain the practical hardness value, which apprehends a good compromise between enhanced mechanical features and effective physical performances. Accomplishments for

such materials promote them as good candidates that are devoted to manufacture efficient devices, for instance, solar cells, among other applications.

## CRediT authorship contribution statement

**Z. Benzarti:** Conceptualization, Methodology, Investigation, Writing - original draft, Writing - review & editing. **T. Sekrafi:** Methodology, Investigation, Writing - original draft. **A. Khalfallah**: Methodology, Investigation, Writing - original draft, Writing - review & editing. **Z. Bougrioua:** Resources, Methodology, **D. Vignaud:** Resources, Methodology, **M. Evaristo:** Resources, Methodology. **A. Cavaleiro:** Resources, Methodology.

## Declaration of Competing Interest

The authors declare that they have no known competing financial interests or personal relationships that could have appeared to influence the work reported in this paper.

## Acknowledgements

The third author A. Khalfallah gratefully acknowledge his support by FEDER funds through the program COMPETE – Programa Operacional Factores de Competitividade – and by national funds through FCT – Fundação para a Ciência e a Tecnologia, under the project UID/EMS/00285/2020. It was also supported by the project RDFORMING (reference PTDC/EMEEME/31243/2017), co-funded by Portuguese Foundation for Science and Technology, by FEDER, through the program Portugal-2020 (PT2020), and by POCI, with reference POCI-01-0145-FEDER-031243. Both supports are gratefully acknowledged.

## Compliance with ethical standards

The authors declare that they have no known competing financial interests or personal relationships that could have appeared to influence the work reported in this paper.

## References

[1] J.C. Lin, Y.K. Su, S.J. Chang, W.H. Lan, K.C. Huang, W.R. Chen, C.Y. Huang, W.C. Lai, W.J. Lin, Y.C. Cheng, High responsivity of GaN p-i-np-i-n photodiode by using low-temperature interlayer, Appl. Phys. Lett. 91 (2007) 173502.
[2] C.J. Neufeld, N.G. Toledo, S.C. Cruz, M. Iza, S.P. DenBaars, U.K. Mishra, High quantum efficiency InGaN/GaN solar cells with 2.95 eV band gap, Appl. Phys. Lett. 93 (2008) 143502.
[3] N.G. Toledo, U.K. Mishra, InGaN solar cell requirements for highefficiency integrated III-nitride/non-III-nitride tandem photovoltaic devices, J. Appl. Phys. 111 (2012) 114505.
[4] Z. Benzarti, T. Sekrafi, Z. Bougrioua, A. Khalfallah, B. El Jani, Effect of SiN treatment on optical properties of InxGa1-xN/GaN MQW blue LEDs, J. Electron. Mater. 46 (2017) 4312–4320.
[5] V.Y. Davydov, A.A. Klochikhin, R.P. Seisyan, V.V. Emtsev, S.V. Ivanov, F. Bechstedt, J. Furthmüller, H. Harima, A.V. Mudryi, J. Aderhold, O. Semchinova, Absorption and emission of hexagonal InN. Evidence of narrow fundamental band gap, Phys. Stat. Sol. B 229 (2002) R1–R3.
[6] J. Wu, W. Walukiewicz, K.M. Yu, J.W. Ager III, E.E. Haller, H. Lu, W.J. Schaff, Y. Saito, Y. Nanishi, Unusual properties of the fundamental band gap of InN, Appl. Phys. Lett. 80 (2002) 3967–3969.
[7] J. Wu, W. Walukiewicz, W. Shan, K.M. Yu, J.W. Ager III, E.E. Haller, H. Lu, W.J. Schaff, Effects of the narrow band gap on the properties of InN, Phys. Rev. B 66 (2002) 201403.
[8] C. Liu, J. Li, The explanation of InN bandgap discrepancy based on experiments and first-principle calculations, Phys. Lett. A 375 (2011) 1152–1155.
[9] A.G. Bhuiyan, A. Hashimoto, A. Yamamoto, Indium nitride (InN): a review on growth, characterization, and properties, J. Appl. Phys. 94 (2003) 2779–2808.
[10] T.L. Tansley, C.P. Foley, Optical band gap of indium nitride, J. Appl. Phys. 59 (1986) 3241–3244.
[11] W. Walukiewicz, S.X. Li, J. Wu, K.M. Yu, J.W. Ager III, E.E. Haller, H. Lu, W.J. Schaff, Optical properties and electronic structure of InN and In-rich group III-nitride alloys, J. Cryst. Growth 269 (2004) 119–127.
[12] T.S. Moss, The interpretation of the properties of indium antimonide, Proc. Phys. Soc. Lond. Sect. B 67 (1954) 775–782.
[13] E. Burstein, Anomalous optical absorption limit in InSb, Phys. Rev. 93 (1954) 632–633.
[14] X.Q. Wang, S.B. Che, Y. Ishitani, A. Yoshikawa, Effect of epitaxial temperature on N-polar InN films grown by molecular beam epitaxy, J. Appl. Phys. 99 (2006) 073512.
[15] P. Schley, R. Goldhahn, G. Gobsch, M. Feneberg, K. Thonke, X. Wang, A. Yoshikawa, Influence of strain on the band gap energy of wurtzite InN, Phys. Stat. Sol. B 246 (2009) 1177–1180.
[16] A. Bchetnia, A. Touré, T.A. Lafford, M.M. Habchi, B. El Jani, Effect of thickness on structural and electrical properties of GaN films grown on SiN-treated sapphire, J. Cryst. Growth 308 (2007) 283–289.
[17] I. Halidou, Z. Benzarti, H. Fitouri, W. Fathallah, B. El Jani, GaN property evolution at all stages of MOVPE Si/N treatment growth, Phys. Stat. Sol. C 4 (2007) 129–132.
[18] Z. Benzarti, I. Halidou, O. Tottereau, T. Boufaden, B. El Jani, Silicon effect on GaN surface morphology, Microelectron. J. 33 (2002) 995–998.
[19] S.Y. Kuo, W.C. Chen, C.C. Kei, C.N. Hsiao, Fabrication of nanostructured indium nitride by PA-MOMBE, Semicond. Sci. Technol. 23 (2008) 055013.
[20] O.A. Laboutin, R.E. Welser, Impact of GaN buffer layer on the growth and properties of InN islands, Appl. Phys. Lett. 92 (2008) 223103.
[21] Y. Nanishi, Y. Saito, T. Yamaguchi, RF-molecular beam epitaxy growth and properties of inn and related alloys, Jpn. J. Appl. Phys. 42 (2003) 2549–2559.
[22] T. Ive, O. Brandt, M. Ramsteiner, M. Giehler, H. Kostial, K.H. Ploog, Properties of InN layers grown on 6H–SiC (0001) by plasma-assisted molecular beam epitaxy, Appl. Phys. Lett. 84 (2004) 1671–1673.
[23] K. Xu, A. Yoshikawa, Effects of film polarities on InN growth by molecular-beam epitaxy, Appl. Phys. Lett. 83 (2003) 251–253.
[24] K. Wang, T. Araki, M. Takeuchi, E. Yoon, Y. Nanishi, Selective growth of N-polar InN through an in situ AlN mask on a sapphire substrate, Appl. Phys. Lett. 104 (2014) 032108.
[25] Y. Zhang, T. Kimura, K. Prasertusk, T. Iwabuchi, S. Kumar, Y. Liu, R. Katayama, T. Matsuoka, Optical properties of InN films grown by pressurized-reactor metalorganic vapor phase epitaxy, Thin Solid Films 536 (2013) 152–155.
[26] I. Yonenaga, Y. Ohkubo, M. Deura, K. Kutsukake, Y. Tokumoto, Y. Ohno, A. Yoshikawa, X.Q. Wang, Elastic properties of indium nitrides grown on sapphire substrates determined by nano-indentation: in comparison with other nitrides, AIP Adv. 5 (2015) 077131.
[27] S.-R. Jian, C.-Y. Huang, W.-C. Ke, Nanoindentation responses of InN thin films, J. Alloy. Compd. 609 (2014) 125–128.
[28] M.A. Hafez, M.A. Mamun, A.A. Elmustafa, H.E. Elsayed-Ali, Structural and nanomechanical properties of InN films grown on Si(1 0 0) by femtosecond pulsed laser deposition, J. Phys. D Appl. Phys. 46 (2013) 175301–175308.
[29] A. Yamamoto, Y. Murakami, K. Koide, M. Adachi, A. Hashimoto, Growth temperature dependences of MOVPE InN on sapphire substrates, Phys. Stat. Sol. B 228 (2001) 5–8.
[30] C.S. Gallinat, G. Koblmüller, F. Wu, J.S. Speck, Evaluation of threading dislocation densities in In- and N-face InN, J. Appl. Phys. 107 (2010) 053517-05323.
[31] G.K. Williamson, W.H. Hall, X-ray line broadening from filed aluminium and wolfram, Acta Metall. 1 (1953) 22–31.
[32] W.C. Oliver, G.M. Pharr, An improved technique for determining hardness and elastic modulus using load and displacement sensing indentation experiments, J. Mater. Res. 7 (1992) 1564–1583.
[33] Y. Huang, H. Wang, Q. Sun, J. Chen, D.Y. Li, J.C. Zhang, J.F. Wang, Y.T. Wang, H. Yang, Evolution of mosaic structure in InN grown by metalorganic chemical vapor deposition, J. Cryst. Growth 293 (2006) 269–272.
[34] Y.-H. Wang, W.-L. Chen, M.-F. Chen, Characterization of InN epilayers grown on Si (111) substrates at various temperatures by MBE, Phys. E 41 (2009) 1746–1751.
[35] Y. Zhang, Y. Liu, T. Kimura, M. Hirata, K. Prasertusk, S. Ji, R. Katayama, T. Matsuoka, Effect of growth temperature on structure properties of InN grown by pressurized-reactor metalorganic vapor phase epitaxy, Phys. Stat. Sol. C 8 (2011) 482–484.
[36] H. Lu, W.J. Schaff, J. Hwang, H. Wu, W. Yeo, A. Pharkya, L.F. Eastman, Improvement on epitaxial grown of InN by migration enhanced epitaxy, Appl. Phys. Lett. 77 (2000) 2548–2550.
[37] X. Wang, S.-B. Chie, Y. Ishitani, A. Yoshikawa, Step-flow growth of In-polar InN by molecular beam epitaxy, Jpn. J. Appl. Phys. 45 (2006) L730–L733.
[38] J. Chaudhuri, J.T. George, D.D. Kolske, A.E. Wickenden, R.L. Henry, Z. Rek, Reduction of dislocation density in GaN films on sapphire using AlN interlayers, J. Mater. Sci. 37 (2002) 1449–1453.
[39] Y.-Y. Wong, E.Y. Chang, T.-H. Yang, J.-R. Chang, Y.-C. Chen, J.-T. Ku, C.-T. Lee, C.-W. Chang, The effect of AlN buffer growth parameters on the defect structure of GaN grown on sapphire by plasma-assisted molecular beam epitaxy, J. Cryst. Growth 311 (2009) 1487–1492.
[40] B. Liu, R. Zhang, Z.L. Xie, H. Lu, Q.J. Liu, Z. Zhang, Y. Li, X.Q. Xiu, P. Chen, P. Han, S.L. Gu, Y. Shi, Y.D. Zheng, W.J. Schaff, Microstructure and dislocation of epitaxial InN films revealed by high resolution x-ray diffraction, J. Appl. Phys. 103 (2008) 023504.
[41] V. Srikant, J.S. Speck, D.R. Clarke, Mosaic structure in epitaxial thin films having large lattice mismatch, J. Appl. Phys. 82 (1997) 4286–4295.
[42] C.G. Dunn, E.F. Koch, Comparison of dislocation densities of primary and secondary recrystallization grains of Si-Fe, Acta Metall. 5 (1957) 548–554.
[43] E. Dimakis, E. Iliopoulos, K. Tsagaraki, A. Adikimenakis, A. Georgakilas, Biaxial strain and lattice constants of InN (0001) films grown by plasma-assisted molecular beam epitaxy, Appl. Phys. Lett. 88 (2006) 191918.

[44] P.F. Fewster, X-ray and neutfon dynamical diyraction: theory and applications, Int. Sch. Crystallogr. 23rd Course (1996) 287.
[45] V. Darakchieva, K. Lorenz, M.–Y. Xie, E. Alves, W.J. Schaff, T. Yamaguchi, Y. Nanishi, S. Ruffenach, M. Moret, O. Briot, Unintentional incorporation of H and related structural and free-electron properties of c- and a-plane InN, Phys. Stat. Sol. A 209 (2012) 91–94.
[46] E. Dimakis, J.Z. Domagala, A. Delimitis, Ph. Komninou, A. Adikimenakis, E. Iliopoulos, A. Georgakilas, Structural properties of 10 μm thick InN grown on sapphire (0001), Superlattices Microstruct. 40 (2006) 246–252.
[47] K.K. Madapu, S. Dhara, Effect of strain relaxation and the Burstein–Moss energy shift on the optical properties of InN films grown in the self-seeded catalytic process, CrystEngComm 18 (2016) 3114–3123.
[48] J. Arvanitidis, D. Christofilos, G.A. Kourouklis, A. Delimitis, M. Katsikini, Ph. Komninou, S. Ves, E. Dimakis, A. Georgakilas, Depth profile of the biaxial strain in a 10 μm thick InN (0001) film, J. Appl. Phys. 100 (2006) 113516.
[49] S. Suihkonen, J. Sormunen, V.T. Rangel-Kuoppa, H. Koskenvaara, M. Sopanen, Growth of InN by vertical flow MOVPE, J. Cryst. Growth 291 (2006) 8–11.
[50] C.S. Gallinat, G. Koblmüller, J.S. Brown, S. Bernardis, J.S. Speck, G.D. Chern, E.D. Readinger, H. Shen, M. Wraback, In-polar InN grown by plasma-assisted molecular beam epitaxy, Appl. Phys. Lett. 89 (2006) 032109–032111.
[51] W. Liu, R.J.N. Tan, C.B. Soh, S.J. Chua, The effects of cap layers on electrical properties of indium nitride films, Appl. Phys. Lett. 97 (2010) 042110.
[52] F.-I. Lai, S.-Y. Kuo, W.-C. Chen, W.-T. Lin, W.-L. Wang, L. Chang, C.-N. Hsiao, C.-H. Chiang, Heteroepitaxial growth of InN on GaN intermediate layer by PA-MOMBE, J. Cryst. Growth 326 (2011) 37–41.
[53] H. Lu, W.J. Schaff, J. Hwang, H. Wu, W. Yeo, A. Pharkya, L.F. Eastman, Improvement on epitaxial grown of InN by migration enhanced epitaxy, Appl. Phys. Lett. 77 (2000) 2548–2550.
[54] K. Wang, Y. Cao, J. Simon, J. Zhang, A. Mintairov, J. Merz, D. Hall, T. Kosel, D. Jena, Effect of dislocation scattering on the transport properties of InN grown on GaN substrates by molecular beam epitaxy, Appl. Phys. Lett. 89 (2006) 162110.
[55] D.Y. Song, M.E. Holtz, A. Chandolu, A. Bernussi, S.A. Nikishin, M.W. Holtz, I. Gherasoiu, Effect of stress and free-carrier concentration on photo-luminescence in InN, Appl. Phys. Lett. 92 (2008) 121913.
[56] H.-C. Wen, W.-C. Chou, T.-Y. Chiang, Y.-R. Jeng, W.-C. Fan, Using nanoindentation and cathodoluminescence to identify the bundled effect of gallium nitride grown by PA-MBE, J. Alloy. Compd. 693 (2017) 615–621.
[57] X.D. Li, H.S. Gao, C.J. Murphy, L.F. Gou, Nanoindentation of silver nanowires, Nano Lett. 4 (2004) 1903–1907.
[58] S. Kataria, T.-W. Liu, C.-L. Hsiao, S. Dhara, L.-C. Chen, K.-H. Chen, S. Dash, A.K. Tyagi, Growth orientation dependent hardness for epitaxial wurtzite InN films, J. Nanosci. Nanotechnol. 10 (2010) 5170–5174.
[59] Y. Ohkubo, M. Deura, Y. Tokumoto, K. Kutsukake, Y. Ohno, I. Yonenaga, Hardness and Young's modulus of InN, IEICE Tech. Rep. 114 (2014) 45–48.